ACS Photonics

pubs.acs.org/journal/apchd5

Article

Violation of Kirchhoff's Law of Thermal Radiation with Space−Time Modulated Grating

Alok Ghanekar,* Jiahui Wang, Shanhui Fan, and Michelle L. Povinelli

Cite This: *ACS Photonics* 2022, 9, 1157−1164

Read Online

ACCESS | Metrics & More | Article Recommendations

ABSTRACT: We present an infrared thermal emitter that exhibits unequal emissivity and absorptivity for a given frequency and angle of incidence, violating Kirchhoff's law of thermal radiation. We exploit spatio-temporal modulation of the refractive index of a grating to drive photonic transitions between guided resonance modes. We show via simulations that the modulation results in directional-dependent reflection. Using a generalized law of thermal radiation valid in the presence of mode conversion, we directly calculate absorptivity and emissivity for our structures. We show that a strong contrast between absorptivity and emissivity can be obtained close to a wavelength of 3.6 μm for realistic modulation frequencies of 10s of GHz. Furthermore, we show that for strong modulation, the system exhibits directional Rabi splitting, giving rise to a stronger contrast between emissivity and absorptivity. The results thus predict the feasibility of nonreciprocal infrared thermal emission without the use of magneto-optical materials.

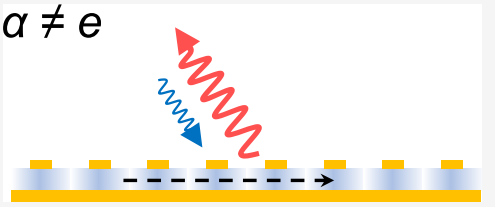

KEYWORDS: *nonreciprocal emissivity, photonic transitions, dynamic modulation, thermal radiation, guided modes*

Naturally occurring thermal radiation is incoherent, broadband, diffuse, and reciprocal.[1−3] In contrast, research on metamaterials has demonstrated the engineering of thermal radiation with defined spectral,[4−6] directional,[7−10] and dynamic[11−14] characteristics, along with phase and polarization control.[15−17] More recently, the case of nonreciprocal thermal radiation has begun to receive considerable attention.[18,19] Materials with nonreciprocal thermal radiation have an emissivity and absorptivity that are not equal for a given frequency and angle of incidence, showing a violation of Kirchhoff's law. In addition to their fundamental interest, nonreciprocal thermal emitters may also provide new approaches to applications, including infrared sensing and energy harvesting.[20−23]

To achieve violation of Kirchhoff's law, Lorentz reciprocity must be broken.[24,25] There are two main approaches to breaking Lorentz reciprocity. One is to use magneto-optical materials, for which the permittivity tensor is asymmetric in the presence of a strong magnetic field.[18,26−28] The second is to use dynamic modulation of the refractive index.[29−33] Previous work has demonstrated the use of dynamic modulation in transmission, reflection, and scattering, resulting in designs for optical isolators[34,35] and circulators.[36] Theoretical analysis of nonreciprocal scattering has illuminated how dynamic index modulation drives the transition between photonic modes,[36−41] creating a highly directional response. In the MHz regime, Hadad et al.[42] demonstrated a nonreciprocal, radiofrequency antenna. This design, which has different angular responses for the transmit and receive functions, suggests intriguing possibilities for exploration at other wavelengths. However, to date, a fully rigorous calculation of the absorptivity and emissivity of a nonreciprocal emitter relying on dynamic modulation has not been performed.

In this work, we design a nonreciprocal, infrared thermal emitter relying on dynamic modulation. We first introduce a general approach for the calculation of absorptivity and emissivity in dynamically modulated systems with mode conversion. We show that the absorptivity at a given incidence angle and wavelength is related to a forward scattering problem, while emissivity is related to an inverse problem. We then introduce a specific semiconductor grating design that supports guided resonance modes and use numerical simulations to model photonic transitions. We show that in the absence of loss, the grating exhibits perfect, nonreciprocal reflection. In the presence of loss, absorptivity and emissivity are unequal, violating Kirchhoff's law. In a stronger modulation regime, we observe the preservation of nonreciprocal scattering and the emergence of Rabi splitting in the forward scattering problem. This results in an even stronger violation of Kirchhoff's law. This work thus establishes a vision for nonreciprocal thermal emitters in dynamically modulated

Received: September 3, 2021
Published: March 11, 2022

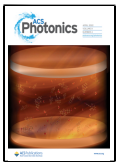

https://doi.org/10.1021/acsphotonics.1c01350
ACS Photonics 2022, 9, 1157−1164

semiconductors, opening up exciting possibilities for both fundamental science and applications.

We start by developing the appropriate formalism for calculations of absorptivity and emissivity in modulated, nonreciprocal systems. To calculate the emissivity for an object with a dielectric constant that is modulated in space and time, we use a generalized modal law of thermal radiation.[43] This approach accurately captures the difference in absorptivity and emissivity for nonreciprocal objects. Consider an optical object O that couples to n free-space ports (Figure 1). We assume that each port is characterized by a frequency ω_n and a wave vector $\boldsymbol{k}_n$, where incoming and outgoing waves propagate with $+\boldsymbol{k}_n$ and $-\boldsymbol{k}_n$, respectively. The modal amplitudes of the waves are indicated by s_{n+} and s_{n-}. The set of free-space modes is assumed to be orthogonal. It is also taken to be complete: we assume that the output wave generated by an input wave at a port s_{n+} can be expressed as a combination of output waves at all ports considered, and an output wave at s_{n-} can be generated by a combination of all input waves considered. In the discussion below, we will restrict our attention to object O with a linear dielectric function that is modulated in space and time and can therefore be viewed as a mode converter.[44] Such a system can be described by a linear relationship between input and output port amplitudes and the S-matrix of the system:

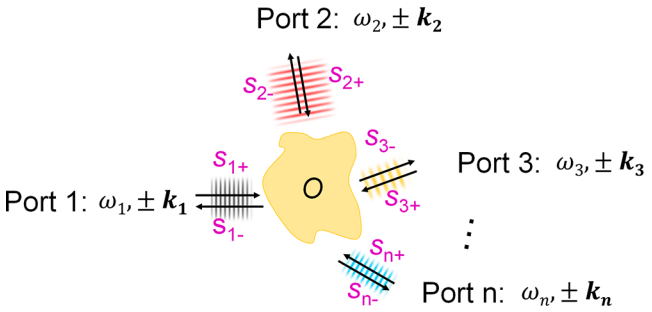

Figure 1. An object O exchanges energy with various modal ports at frequencies ω_1, ω_2, ω_3, ..., ω_n, wave vectors $\boldsymbol{k}_1$, $\boldsymbol{k}_2$, $\boldsymbol{k}_3$, ..., $\boldsymbol{k}_n$, and modal amplitudes s_1, s_2, s_3, ..., s_n.

$$\begin{bmatrix} s_{1-} \\ s_{2-} \\ \vdots \\ s_{n-} \end{bmatrix} = \begin{bmatrix} S_{11} & S_{12} & \cdots & S_{1n} \\ S_{21} & \ddots & & \\ \vdots & & \ddots & \\ S_{n1} & \cdots & \cdots & S_{nn} \end{bmatrix} \begin{bmatrix} s_{1+} \\ s_{2+} \\ \vdots \\ s_{n+} \end{bmatrix} \tag{1}$$

Following ref 43, the absorptivity matrix A and emissivity matrix E are related to the scattering matrix of the system S by

$$A = I_I - S^{\dagger}S \tag{2}$$

and

$$E = I_O - SS^{\dagger} \tag{3}$$

Here, I_I and I_O are identity matrices in input and output space, respectively, and † represents conjugate-transpose. The absorptivity (α_p) and emissivity (e_p) values at a particular port p are given by the diagonal elements of the A and E matrices, i.e., $\alpha_p = A_{pp}$ and $e_p = E_{pp}$,[43] which can be written as

$$\alpha_p = 1 - \sum_q |S_{qp}|^2 \tag{4}$$

and

$$e_p = 1 - \sum_q |S_{pq}|^2 \tag{5}$$

The formalism of eqs 2−5 was originally derived for time-independent systems based on the principle of conservation of energy.[43] In a space−time modulated system, energy conservation no longer applies. However, photon flux is conserved during frequency-conversion processes, as described by the Manley−Rowe relation.[34,45] Moreover, the definition of

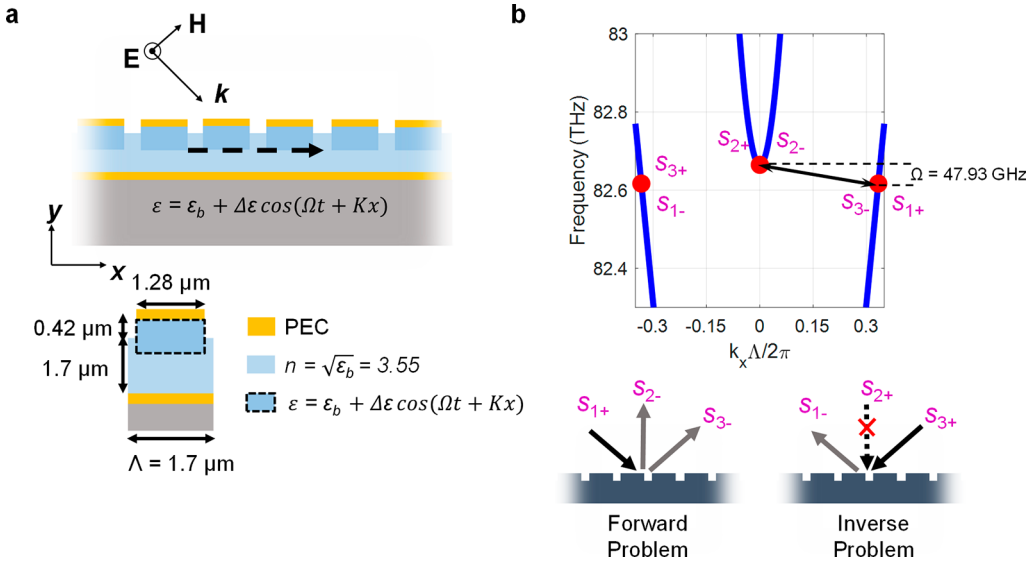

Figure 2. Schematics of the proposed design: (a) guided mode resonance grating design and corresponding unit cell. The dashed region undergoes time-dependent modulation of the refractive index. (b) Calculated band structure of the grating, highlighting resonant modes of interest. Modes excited by s_{1+} and s_{2+} are separated by modulation frequency $\Omega = 47.93$ GHz and normalized wave vector $K\Lambda/2\pi = +1/3$. Forward problem: modes excited by obliquely incident wave s_{1+} can couple to outgoing waves s_{2-} and s_{3-}. Inverse problem: an outgoing wave s_{1-} can result only from input wave s_{3+}.

https://doi.org/10.1021/acsphotonics.1c01350
ACS Photonics 2022, 9, 1157−1164

a mode-converter basis set remains valid for a system varying in space and time.[44] Therefore, eqs 4 and 5 remain valid when defined for steady-state photon flux.

In particular, the absorptivity and emissivity must be defined in terms of photon flux, rather than power. For a port p at frequency ω and angle of incidence θ, the absorptivity (α_p) is defined as

$$\alpha_p = \frac{\Phi_{abs}}{\Phi_{inc}} \tag{6}$$

where Φ_{abs} is the absorbed photon flux and Φ_{inc} is the incident photon flux. Similarly, emissivity into port p can be defined as

$$e_p = \frac{\Phi_{emit}}{\Phi_{BB}} \tag{7}$$

where Φ_{emit} is the photon number flux emitted by the object into port p (at frequency ω and angle θ), and Φ_{BB} is the photon number flux emitted by a blackbody at the same temperature, wavelength, and angle.

The scattering matrix element S_{pq} for input port q and output port p is also defined in terms of the photon flux:

$$|S_{pq}|^2 = \frac{\Phi_p}{\Phi_q} \tag{8}$$

Here, Φ_p and Φ_q are the photon fluxes at output port p and input port q, respectively, corresponding to frequencies ω_p and ω_q. When the modulation frequency Ω is much smaller than the operational frequency ω_0, the ratio of photon fluxes is nearly identical to the ratio of power fluxes.

Nonreciprocity has important consequences for the relationship between absorptivity and emissivity at a particular frequency and incident angle. For a nonreciprocal object, the scattering matrix is asymmetric: $S \neq S^T$ ($S_{qp} \neq S_{pq}$). From eqs 4 and 5, we see that the formulas for absorptivity and emissivity involve different sums over the scattering matrix elements. Below, we will show that α_p and e_p can be unequal for dynamically modulated systems with loss, leading to violation of Kirchhoff's law.

To illustrate how nonreciprocity can be induced by a traveling-wave index modulation,[36] we consider a guided-mode resonance grating. Our design is shown in Figure 2a. It consists of a dielectric grating coated with a perfect electrical conductor (PEC) on the top and bottom surfaces. A detail of the unit cell is shown below the grating. The real part of the refractive index of the dielectric (n) is taken to be 3.55 (e.g., similar to InAs at 3.6 μm). We consider transverse electric (TE) polarization, where only the z-component of the electric field is nonzero. The region highlighted by the dashed line undergoes a spatio-temporal permittivity modulation represented by $\varepsilon = \varepsilon_b + \Delta\varepsilon \cos(\Omega t + Kx)$. Here, ε_b is the base permittivity of the dielectric, $\Delta\varepsilon$ is the amplitude of modulation, Ω is the modulation frequency, and K is the spatial frequency of modulation. $\delta = \Delta\varepsilon/\varepsilon_b$ is defined as the modulation depth. For zero modulation depth, we calculate the band structure of the grating using COMSOL and plot the results in Figure 2b. The parallel wave vector is shown in normalized units $k_x\Lambda/2\pi$, while the frequency is shown in real units of THz.

To calculate the absorptivity of a given port, we first examine the forward problem, shown in the bottom left of Figure 2b. Consider an incident wave s_{1+} in free space with a wave vector $k_x\Lambda/2\pi = +1/3$, which corresponds to an incident angle of approximately +45.36° and an angular frequency $\omega_0 = 2\pi \times 82.617$ THz. The incoming wave will couple to a mode of the grating with the same k_x and ω_0, indicated by the rightmost dot on the band structure of Figure 2b. In the absence of modulation and loss, the outgoing wave will exit into port 3 with $|s_{3-}| = |s_{1+}|$. Since the period of the grating is smaller than the wavelength (3.628 μm), diffraction into higher orders does not occur. Modulation introduces coupling between modes of the grating, as indicated by the black arrow on the band structure. Here, we have chosen a modulation frequency $\Omega = 2\pi \times 47.93$ GHz and spatial frequency $K\Lambda/2\pi = +1/3$, for which the modulation repeats every three periods of the grating. The coupling allows some light to exit the grating at normal incidence into port 2. The corresponding wave vector and angular frequency are $k_x\Lambda/2\pi = 0$ and $\omega_0 + \Omega$, respectively. From eq 3, the calculation of absorptivity for port 1 (α_1) will involve both scattering from port 1 to port 2 (scattering matrix element S_{21}) and that from port 1 to port 3 (S_{31}).

To calculate the emissivity of a given port, we consider an inverse problem, shown in the bottom right of Figure 2b. In this case, we must identify all input ports that can produce output at port 1. In the absence of modulation, an incident wave at port 3 with amplitude s_{3+} will reflect from the grating into s_1. In the presence of modulation, we might consider whether an input s_{2+} at port 2 can also produce output at port 1. The calculation of emissivity for port 1 would then include both processes (corresponding to matrix elements S_{12} and S_{13}). However, light incident from port 2 at $k_x\Lambda/2\pi = 0$ and $\omega_0 + \Omega$ actually cannot convert to s_{1-} at ω_0 due to phase mismatch. Qualitatively, this is because the modulation vector (black arrow in Figure 2b) has the wrong slope to be able to connect the two points (s_{2+} and s_{1-}). Below, we show quantitatively that the corresponding scattering matrix element (S_{12}) is equal to zero. The dashed arrow and red "x" in Figure 2b highlights that the s_{2+} to s_{1-} conversion process does not occur.

We note that in standard grating theory, a common convention is to define separate scattering matrices for a Bloch wave vector k_x and its mirror image $-k_x$,[46,47] since modes at these two wave vectors in most cases do not couple with each other. Within our formalism (eq 1), since the dynamic modulation may couple grating modes with opposite wave vectors together, we use a scattering matrix to describe all modes that may be coupled together by the dynamic modulation. For example, in our scattering matrix, both s_{1+} and s_{3+} are included, and these modes have opposite Bloch wave vectors.

To calculate the numerical values of the scattering matrix elements, we use a multifrequency, finite-difference frequency-domain (FDFD) method.[36,48] In comparison with time-domain simulations of photonic transitions,[34] this approach greatly shortens the computation time for systems in which the modulation period is much longer than the optical period. We simulate the fields at frequencies $\omega_0 \pm \Omega$, $\omega_0 \pm 2\Omega$, and $\omega_0 \pm 3\Omega$, in addition to the field at the excitation frequency ω_0. Each time-harmonic field is represented by a separate physics node in COMSOL Multiphysics simulation. The refractive index modulation is modeled using current-density terms, which couples the different time harmonics as in ref 48. We considered 3-unit periods to simulate the modulated grating. The $\cos(Kx)$ spatial dependence of the modulation is simplified by taking the phase to be constant within a single modulation region (dashed rectangle in Figure 2a) and

https://doi.org/10.1021/acsphotonics.1c01350
ACS Photonics 2022, 9, 1157−1164

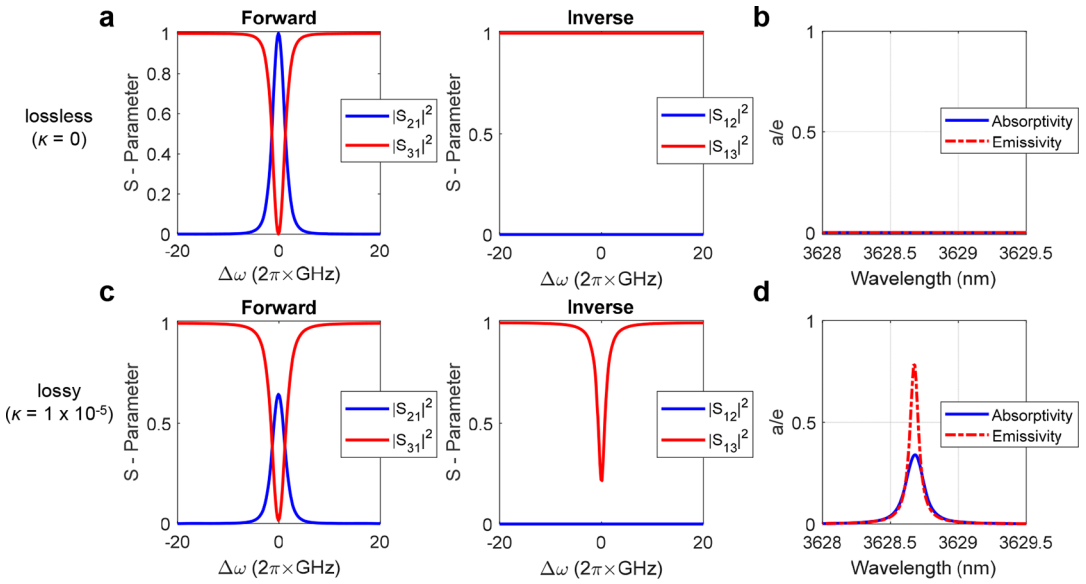

Figure 3. Spectrum of *S*-parameters and calculated emissivity/absorptivity for the critically coupled system with $\delta = 2.33 \times 10^{-4}$: (a) lossless system showing complete nonreciprocal mode conversion. (b) No emission or absorption is seen due to the absence of loss. (c) Weaker conversion is observed with introduction of loss. (d) Unequal absorptivity and emissivity are seen as a violation of Kirchhoff's law.

imposing a phase difference of $\varphi = K\Lambda$ between adjacent modulation regions or unit cells. Floquet periodic boundary conditions are used for all time harmonics. With a choice of modulation phase φ of $2\pi/3$, the phase difference between the boundaries is a multiple of 2π.

We first consider *S*-parameters for the system with no loss. From previous work on nonreciprocal reflectors,[36] we expect that for a lossless system, there will be a value of the modulation depth for which complete conversion from s_{1+} to s_{2-} occurs, a condition known as critical coupling. For our system, we determined numerically that the modulation depth for critical coupling is $\delta = 2.33 \times 10^{-4}$. In Figure 3a, we plot the *S*-parameters at critical coupling as a function of detuning frequency $\Delta\omega$, where $|S_{pq}(\Delta\omega)|^2 \equiv N_q(\omega_q + \Delta\omega)/N_p(\omega_p + \Delta\omega)$. We observe that $|S_{31}|^2$ goes to zero at $\Delta\omega = 0$, while $|S_{13}|^2 \equiv 1$ for all frequencies. This indicates that the reflection from the structure is strongly nonreciprocal. In the forward direction, the specular reflection vanishes on resonance. In the reverse direction, it is equal to 1. This is due to perfect mode conversion in the forward direction ($|S_{21}|^2 = 1$). From Figure 3a, we see that the system exhibits nonreciprocal scattering with $S \neq S^T$.

We can calculate the emissivity and absorptivity for port 1 of the metasurface using the formulation presented in eqs 3 and 4. Figure 3b shows that both the emissivity and absorptivity are zero for all frequencies, as expected for a lossless system. From the plot of the forward case in Figure 3a, we see that $|S_{21}|^2 + |S_{31}|^2 = 1$ for all frequencies. This sum enters the formula in eq 3, resulting in zero absorptivity. For the reverse case in Figure 3a, we see that $|S_{12}|^2 + |S_{13}|^2$ is also equal to 1 for all frequencies, which, from eq 4, results in zero emissivity. Nonreciprocal systems with zero loss do not violate Kirchhoff's law, as both absorptivity and emissivity are identical to zero.

We introduce loss into our system by including a small imaginary part κ in the dielectric refractive index. We set $\kappa = 1 \times 10^{-5}$ inside the blue regions of Figure 2a. The calculated *S*-parameters in the presence of loss are shown in Figure 3c. On resonance, there is a partial conversion of incident light from port 1 to port 2 (the value of $|S_{21}|^2 > 0$). There is no specular reflection ($|S_{31}|^2 = 0$ on resonance), indicating that the remaining, unconverted light is absorbed. The reflection spectrum is slightly broadened due to loss, reducing the *Q*-factor. In the reverse direction, there is a dip in the reflection spectrum ($|S_{13}|^2$) due to resonant absorption. The matrix element $|S_{12}|^2$ is also required for the calculation of emissivity via eq 4 and was found to be zero over all frequencies. The system is clearly nonreciprocal, with $|S_{21}|^2 \neq |S_{12}|^2$ and $|S_{31}|^2 \neq |S_{13}|^2$.

The absorptivity and emissivity in the presence of loss are plotted in Figure 3d. On resonance, absorptivity is larger than the emissivity. This difference arises from the scattering matrix elements shown in Figure 3c. On resonance, the sum of $|S_{21}|^2$ and $|S_{31}|^2$ is larger than $|S_{12}|^2 + |S_{13}|^2$. From Figure 3d, we see that the contrast, defined as $|\alpha\text{-}\epsilon|$, is equal to 0.445 at 3628.68 nm. Physically, this difference corresponds to the difference in absorptivity and emissivity for an incident plane wave at an angle of 45.36°. As we move away from the central wavelength, the contrast decreases. This numerical result provides direct evidence that a nonreciprocal system with loss can strongly violate Kirchhoff's law.

Increasing the modulation depth beyond critical coupling opens up a new physical regime for nonreciprocal scattering. Previous work on strongly modulated media has identified the emergence of scattering to additional space−time harmonics[42] as well as modal splitting.[49] Below, we study how these processes impact nonreciprocal scattering and violations of Kirchhoff's law.

In principle, a modulation with frequency Ω and wave vector K can convert light in an incident mode with wave vector k_{0x} and frequency ω_0 to any other mode of the form $(\omega_0 + n\Omega, k_{0x} - nK)$. In our system, $K\Lambda/2\pi = 1/3$. If we choose an initial mode with $k_{0x} = K$ and $\omega_0 = 2\pi \times 82.617$ THz, as in Figure 2b, we can determine the set of all possible space−time harmonics. These are indicated by red dots in Figure 4a. Notice that there are only three possible values of the wave vector, $k_x = -1/3(2\pi/\Lambda)$, 0, and $1/3(2\pi/\Lambda)$. This occurs due to the wrapping of the Brillouin zone; harmonics with values $k_{0x} + nK$ lying

https://doi.org/10.1021/acsphotonics.1c01350
ACS Photonics 2022, 9, 1157−1164

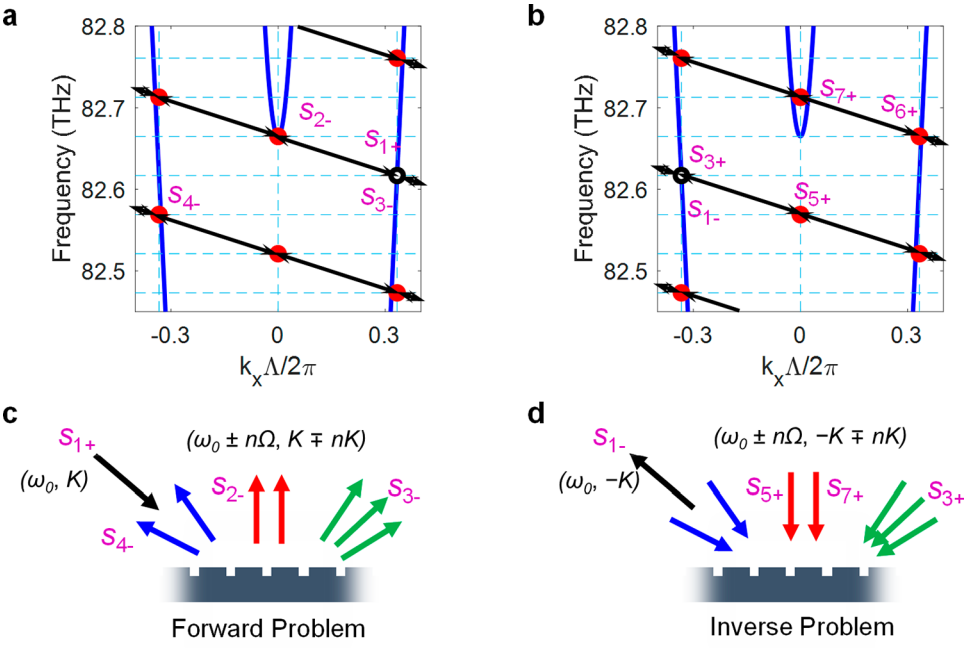

Figure 4. (a) For stronger modulation, additional conversion processes become possible. In principle, the modulation can convert light in an incident mode with wave vector k_{0x} and frequency ω_0 to any other mode of the form $(\omega_0 + n\Omega, k_{0x} - nK)$. Light incident at s_{1+} can couple to a set of modes indicated by red dots that are separated by the modulation vector indicated by arrows. (b) Modes indicated by red dots $(\omega_0 + n\Omega, -k_{0x} - nK)$ that can produce output mode s_{1-}. (c) Schematic of the forward problem displaying incident wave amplitude s_{1+} and multiple, potential output ports, indicated by blue, red, and green arrows. Specific output ports of interest have been assigned indices for convenience and labeled s_{i-}. (d) Inverse problem schematic showing outgoing wave s_{1-} that can be generated by various inputs labeled s_{i+}.

outside of $(-0.5, 0.5)(2\pi/\Lambda)$ are mapped back into the first Brillouin zone by adding or subtracting a multiple of $(2\pi/\Lambda)$.

First, consider the forward problem, wherein light is incident at s_{1+}. Light will couple to the mode of the grating indicated by the small, black circle in Figure 4a. From numerical simulations, we observe that the modulation couples the initial mode to grating modes of the form $(\omega_0 + n\Omega, k_{0x} - nK)$, where n can take both positive and negative values. These modes are indicated by the red dots in Figure 2b and are connected by black arrows representing the modulation, which can wrap around the edges of the Brillouin zone. The grating modes couple to output ports in free space with the same frequency and parallel wave vector.

The forward scattering process is shown schematically in Figure 4c. The light input at s_{1+} can exit the system in the forward, normal, or backward direction. Light in the forward direction contains a component due to specular reflection (s_{3-}), as seen above. It also contains components due to mode conversion, specifically from conversion to modes with wave vectors $= +(1/3)(2\pi/\Lambda)$. Each forward component will exit the grating with a slightly different angle, given by $\theta = \sin^{-1}(ck_x/\omega)$. This is indicated schematically on the grating by the multiple, green arrows. Light exiting the grating at normal incidence arises from conversion to modes at $k_x = 0$. Multiple frequencies are in principle possible (red arrows). From our simulation results below, we find that the strongest output occurs in s_{3-}. Light exiting in the backward direction corresponds to $k_x = +(1/3)(2\pi/\Lambda)$. Again, multiple frequencies, corresponding to slightly different angles, are possible (blue arrows). We label the dominant backward port as s_{4-} for convenience.

The calculation of emissivity requires the consideration of the inverse problem. We must identify all possible input modes that can produce a nonzero output at s_{1-}. This set is indicated by the red dots in Figure 4b. The scattering process is depicted by Figure 4d. As mentioned before, specular reflection couples s_{3+} to s_{1-}. For strong modulation, additional modes can also produce output at s_{1-}, as indicated schematically by the arrows. Modes with green, red, and blue arrows correspond to wave vectors $k_x\Lambda/2\pi = -1/3$, 0, and 1/3, respectively. We note that the set of modes indicated by red dots in Figure 4a,b are distinct.

In Figure 5a, we plot the S-parameters of the strongly modulated system for the case of no loss. A modulation depth $\delta = 2.33 \times 10^{-3}$ was used in simulation. In the forward problem, when light is incident at s_{1+}, the only significant scattering matrix elements $(|S_{pq}|^2 > 1 \times 10^{-3})$ were S_{21}, S_{31}, and S_{41}, corresponding to output at s_{2-}, s_{3-}, and s_{4-}. The grating modes that couple to each of these output ports are labeled in Figure 4b for convenience. Clear mode splitting is observed in the spectrum. The spectrum is asymmetric around the center frequency. In the inverse problem, the input at port 3, 5, 6, or 7 produces a strong output at port 1, corresponding to significant scattering elements S_{13}, S_{15}, S_{16}, and S_{17}. No splitting is observed in the inverse spectrum. The peak is shifted slightly above the center frequency. The nonreciprocal character of the grating is clearly illustrated by comparing $|S_{31}|^2$ and $|S_{13}|^2$, which are clearly different in both shape and magnitude. The absorptivity and emissivity are plotted in Figure 5b and are equal to zero, as required for a lossless system.

Figure 5c shows the S-parameters for the strongly modulated system with a loss value of $\kappa = 1 \times 10^{-5}$. Similar to the lossless case, the forward problem exhibits spectral splitting, while the inverse problem does not. The nonreciprocal character is evident from the fact that $|S_{13}|^2 \neq |S_{31}|^2$. Figure 5d shows the absorptivity and emissivity for port 1. We observe that the

https://doi.org/10.1021/acsphotonics.1c01350
ACS Photonics 2022, 9, 1157−1164

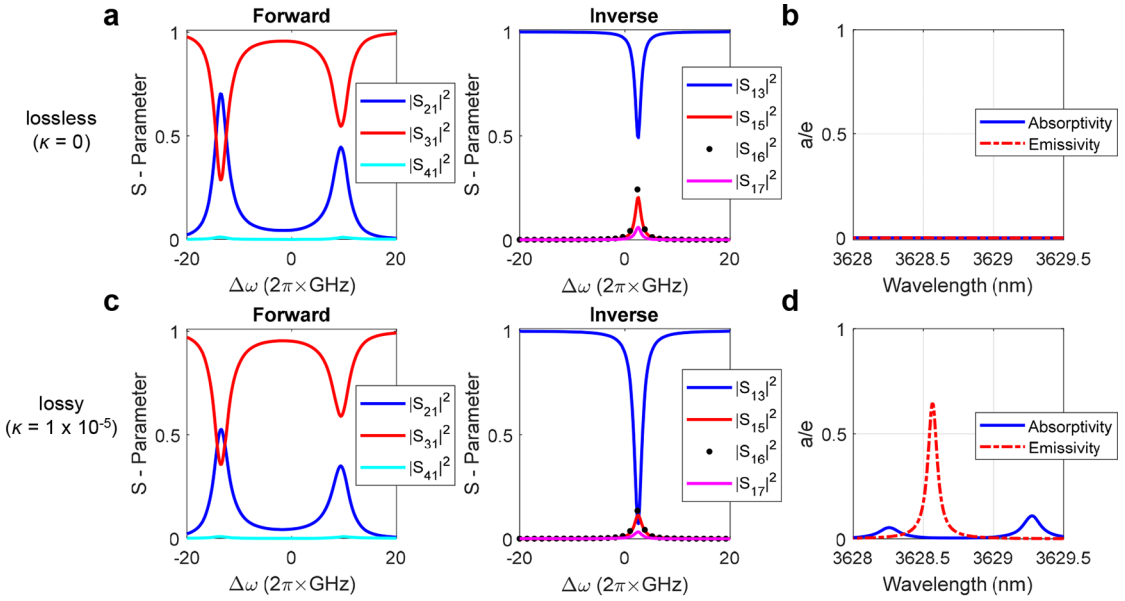

Figure 5. Spectrum of *S*-parameters and corresponding emissivity/absorptivity spectra in strongly modulated regime with $\delta = 2.33 \times 10^{-3}$: (a) lossless system showing nonreciprocal Rabi splitting. The inverse problem also exhibits mode conversion due to strong modulation. (b) The emissivity and absorptivity spectra are zero. (c) A lossy system with $\kappa = 1 \times 10^{-5}$ shows weaker conversion but exhibits a stronger contrast at central frequency owing to loss. (d) A high contrast in emissivity and absorptivity is observed.

absorptivity has an asymmetric, split-peak shape, which originates from the shape of the *S*-matrix spectra for the forward problem. The emissivity has a single peak shape, reflecting the shape of the *S*-matrix spectra for the inverse problem. The contrast $|\alpha - e|$ is maximized at a wavelength of 3628.56 nm, corresponding to an incident angle of 45.36°. This value is larger than for the critical-coupling case.

Directional-dependent splitting of the *S*-matrix elements observed in Figures 4 and 5 has previously been observed in modulated, side-coupled microring systems.[42] We can gain insight into this phenomenon by drawing an analogy between the two systems. The specular reflection path in our system (port 1 → 3) plays an analogous role to forward waveguide transmission without frequency conversion in the side-coupled microring. Floquet analysis shows that a phase-matched modulation induces direction-dependent Rabi splitting.[49] This results in a split-peak spectrum for the forward scattering process (S_{31}) and a single-peak spectrum for the inverse process (S_{13}). As above, we have shown for the first time that this directional dependence of the scattering matrix directly results in the violation of Kirchhoff's law.

The method we used for calculations of absorptivity and emissivity considered a particular input port, corresponding to a specified ω_0 and k_x in free space. Given these values, we can calculate the corresponding wavelength and angle. We note that when interpreting the absorptivity and emissivity spectra of Figures 3d and 5d, the incident angle varies slightly with wavelength as $\theta = \sin^{-1}(\lambda k_x/2\pi)$. This procedure outlined here can be used quite generally to determine absorptivity and emissivity and any given wavelength and angle of interest, provided that the incoming wave couples to a single-guided resonance mode of the structure. This condition will hold in most cases, apart from degenerate points in the band structure. In this case, the relative excitation of the degenerate modes must be determined and used in the coupled side-band simulation method.

We envision that the design of Figure 2a can be implemented in an InAs material system. The refractive index of InAs strongly depends on carrier concentration in the 2.1−4.4 μm wavelength range,[50] allowing for spatial- and time-dependent tuning. The loss values for heavily doped InAs are consistent with the range studied here ($\kappa \approx 1 \times 10^{-5}$).[51] Top and bottom metal contacts could be potentially used for injection tuning.

In conclusion, we proposed a design of a nonreciprocal infrared thermal emitter based on a dynamically modulated, guided-resonance mode grating. We developed a framework for calculating the absorptivity and emissivity of the structure from the scattering matrix that is valid for systems with mode conversion. We present a specific grating design that exhibits asymmetric directional reflection at an oblique angle of incidence. For a modulation depth corresponding to critical coupling, we show that directional asymmetry in the scattering matrix results in violations of Kirchhoff's law, with absorptivity not equal to emissivity for a given frequency and angle of incidence. For larger modulation depths, we observe directional-dependent Rabi splitting in the scattering matrix. The forward scattering matrix elements that enter the absorptivity calculation exhibit spectral splitting, resulting in a split-peak absorptivity spectrum. The scattering matrix elements that enter the emissivity do not split, resulting in a single-peak emissivity. This behavior results in a strong contrast (large $|\alpha - e|$) at high modulation depths.

Significantly, this work enables a route to nonreciprocal thermal emission without the use of magneto-optical materials. The concept presented here relies on the dynamic modulation of the refractive index, which can potentially be achieved in a more general class of electro-optic materials. The design is thus the first step toward realizing magnet-free nonreciprocal thermal emitters at designed wavelengths of interest. In addition to being of fundamental importance, the ability to achieve thermally emissive nonreciprocity in realistic, engineered systems may have important applications in energy

https://doi.org/10.1021/acsphotonics.1c01350
ACS Photonics 2022, 9, 1157−1164

harvesting. Traditional approaches to energy harvesting are bounded by the fundamental limits imposed by reciprocity. Nonreciprocal systems may thus enable novel approaches in this field.

AUTHOR INFORMATION

Corresponding Author

Alok Ghanekar − *Ming Hsieh Department of Electrical and Computer Engineering, University of Southern California, Los Angeles, California 90089, United States;* orcid.org/0000-0002-8181-481X; Email: aghaneka@usc.edu

Authors

Jiahui Wang − *Department of Applied Physics, Stanford University, Stanford, California 94305, United States*

Shanhui Fan − *Department of Electrical Engineering, Stanford University, Stanford, California 94305, United States;* orcid.org/0000-0002-0081-9732

Michelle L. Povinelli − *Ming Hsieh Department of Electrical and Computer Engineering, University of Southern California, Los Angeles, California 90089, United States*

Complete contact information is available at: https://pubs.acs.org/10.1021/acsphotonics.1c01350

Funding

This work is funded by Defense Advanced Research Projects Agency (DARPA) grant HR00111820046.

Notes

The authors declare no competing financial interest.

REFERENCES

(1) Orlande, H. R.; Fudym, O.; Maillet, D.; Cotta, R. M., *Thermal measurements and inverse techniques*. CRC Press: 2011, DOI: 10.1201/b10918.

(2) Modest, M. F., *Radiative heat transfer*; Academic press: 2013.

(3) Tilley, D. Thermal Physics (2nd edn). *Physics Bulletin* **1980**, *31*, 321.

(4) Lee, B. J.; Fu, C. J.; Zhang, Z. M. Coherent thermal emission from one-dimensional photonic crystals. *Appl. Phys. Lett.* **2005**, *87*, No. 071904.

(5) Liu, X.; Tyler, T.; Starr, T.; Starr, A. F.; Jokerst, N. M.; Padilla, W. J. Taming the blackbody with infrared metamaterials as selective thermal emitters. *Phys. Rev. Lett.* **2011**, *107*, No. 045901.

(6) Ilic, O.; Bermel, P.; Chen, G.; Joannopoulos, J. D.; Celanovic, I.; Soljačić, M. Tailoring high-temperature radiation and the resurrection of the incandescent source. *Nat. Nanotechnol.* **2016**, *11*, 320−324.

(7) Greffet, J.-J.; Carminati, R.; Joulain, K.; Mulet, J.-P.; Mainguy, S.; Chen, Y. Coherent emission of light by thermal sources. *Nature* **2002**, *416*, 61−64.

(8) Laroche, M.; Arnold, C.; Marquier, F.; Carminati, R.; Greffet, J.-J.; Collin, S.; Bardou, N.; Pelouard, J.-L. Highly directional radiation generated by a tungsten thermal source. *Opt. Lett.* **2005**, *30*, 2623−2625.

(9) Chalabi, H.; Alù, A.; Brongersma, M. L. Focused thermal emission from a nanostructured SiC surface. *Phys. Rev. B* **2016**, *94*, No. 094307.

(10) Inampudi, S.; Mosallaei, H. Tunable wideband-directive thermal emission from SiC surface using bundled graphene sheets. *Phys. Rev. B* **2017**, *96*, 125407.

(11) Brar, V. W.; Sherrott, M. C.; Jang, M. S.; Kim, S.; Kim, L.; Choi, M.; Sweatlock, L. A.; Atwater, H. A. Electronic modulation of infrared radiation in graphene plasmonic resonators. *Nat. Commun.* **2015**, *6*, 7032−7037.

(12) Liu, X.; Padilla, W. J. Dynamic manipulation of infrared radiation with MEMS metamaterials. *Adv. Opt. Mater.* **2013**, *1*, 559−562.

(13) Kats, M. A.; Blanchard, R.; Zhang, S.; Genevet, P.; Ko, C.; Ramanathan, S.; Capasso, F. Vanadium dioxide as a natural disordered metamaterial: perfect thermal emission and large broadband negative differential thermal emittance. *Phys. Rev. X* **2013**, *3*, No. 041004.

(14) Inoue, T.; Zoysa, M. D.; Asano, T.; Noda, S. Realization of dynamic thermal emission control. *Nat. Mater.* **2014**, *13*, 928−931.

(15) Arbabi, A.; Horie, Y.; Bagheri, M.; Faraon, A. Dielectric metasurfaces for complete control of phase and polarization with subwavelength spatial resolution and high transmission. *Nat. Nanotechnol.* **2015**, *10*, 937−943.

(16) Schuller, J. A.; Taubner, T.; Brongersma, M. L. Optical antenna thermal emitters. *Nat. Photonics* **2009**, *3*, 658−661.

(17) Wu, C.; Arju, N.; Kelp, G.; Fan, J. A.; Dominguez, J.; Gonzales, E.; Tutuc, E.; Brener, I.; Shvets, G. Spectrally selective chiral silicon metasurfaces based on infrared Fano resonances. *Nat. Commun.* **2014**, *5*, 3892−3899.

(18) Zhu, L.; Fan, S. Near-complete violation of detailed balance in thermal radiation. *Phys. Rev. B* **2014**, *90*, 220301.

(19) Buddhiraju, S.; Li, W.; Fan, S. Photonic refrigeration from time-modulated thermal emission. *Phys. Rev. Lett.* **2020**, *124*, No. 077402.

(20) Ries, H. Complete and reversible absorption of radiation. *Appl. Phys. B: Lasers Opt.* **1983**, *32*, 153−156.

(21) Green, M. A. Time-asymmetric photovoltaics. *Nano Lett.* **2012**, *12*, 5985−5988.

(22) Polman, A.; Atwater, H. A. Photonic design principles for ultrahigh-efficiency photovoltaics. *Nat. Mater.* **2012**, *11*, 174−177.

(23) Buddhiraju, S.; Fan, S. Theory of solar cell light trapping through a nonequilibrium Green's function formulation of Maxwell's equations. *Phys. Rev. B* **2017**, *96*, No. 035304.

(24) Landau, L. D.; Bell, J.; Kearsley, M.; Pitaevskii, L.; Lifshitz, E.; Sykes, J., *Electrodynamics of continuous media*; elsevier: 2013, Vol. *8*.

(25) Han, S. E. Theory of thermal emission from periodic structures. *Phys. Rev. B* **2009**, *80*, 155108.

(26) Snyder, W. C.; Wan, Z.; Li, X. Thermodynamic constraints on reflectance reciprocity and Kirchhoff's law. *Appl. Opt.* **1998**, *37*, 3464−3470.

(27) Zhu, L.; Fan, S. Persistent directional current at equilibrium in nonreciprocal many-body near field electromagnetic heat transfer. *Phys. Rev. Lett.* **2016**, *117*, 134303.

(28) Zhao, B.; Shi, Y.; Wang, J.; Zhao, Z.; Zhao, N.; Fan, S. Near-complete violation of Kirchhoff's law of thermal radiation with a $_{0.3}$ T magnetic field. *Opt. Lett.* **2019**, *44*, 4203−4206.

(29) Shaltout, A.; Kildishev, A.; Shalaev, V. Time-varying metasurfaces and Lorentz non-reciprocity. *Opt. Mater. Express* **2015**, *5*, 2459−2467.

(30) Hadad, Y.; Sounas, D. L.; Alu, A. Space-time gradient metasurfaces. *Phys. Rev. B* **2015**, *92*, 100304.

(31) Shi, Y.; Fan, S. Dynamic non-reciprocal meta-surfaces with arbitrary phase reconfigurability based on photonic transition in meta-atoms. *Appl. Phys. Lett.* **2016**, *108*, No. 021110.

(32) Taravati, S. Giant linear nonreciprocity, zero reflection, and zero band gap in equilibrated space-time-varying media. *Phys. Rev. Appl.* **2018**, *9*, No. 064012.

(33) Taravati, S.; Kishk, A. A. Space-time modulation: Principles and applications. *IEEE Microwave Magazine* **2020**, *21*, 30−56.

(34) Yu, Z.; Fan, S. Complete optical isolation created by indirect interband photonic transitions. *Nat. Photonics* **2009**, *3*, 91−94.

(35) Lin, Q.; Wang, J.; Fan, S. Compact dynamic optical isolator based on tandem phase modulators. *Opt. Lett.* **2019**, *44*, 2240−2243.

(36) Shi, Y.; Han, S.; Fan, S. Optical circulation and isolation based on indirect photonic transitions of guided resonance modes. *ACS Photonics* **2017**, *4*, 1639−1645.

(37) Dong, P.; Preble, S. F.; Robinson, J. T.; Manipatruni, S.; Lipson, M. Inducing photonic transitions between discrete modes in a silicon optical microcavity. *Phys. Rev. Lett.* **2008**, *100*, No. 033904.

(38) Fang, K.; Yu, Z.; Fan, S. Photonic Aharonov-Bohm effect based on dynamic modulation. *Phys. Rev. Lett.* **2012**, *108*, 153901.

(39) Li, E.; Eggleton, B. J.; Fang, K.; Fan, S. Photonic Aharonov–Bohm effect in photon–phonon interactions. *Nat. Commun.* **2014**, *5*, 3225–3225.
(40) Tzuang, L. D.; Fang, K.; Nussenzveig, P.; Fan, S.; Lipson, M. Non-reciprocal phase shift induced by an effective magnetic flux for light. *Nat. Photonics* **2014**, *8*, 701–705.
(41) Winn, J. N.; Fan, S.; Joannopoulos, J. D.; Ippen, E. P. Interband transitions in photonic crystals. *Phys. Rev. B* **1999**, *59*, 1551.
(42) Hadad, Y.; Soric, J. C.; Alu, A. Breaking temporal symmetries for emission and absorption. *Proc. Natl. Acad. Sci. U. S. A.* **2016**, *113*, 3471–3475.
(43) Miller, D. A. B.; Zhu, L.; Fan, S. Universal modal radiation laws for all thermal emitters. *Proc. Natl. Acad. Sci. U. S. A.* **2017**, *114*, 4336–4341.
(44) Miller, D. A. B. All linear optical devices are mode converters. *Opt. Express* **2012**, *20*, 23985–23993.
(45) Bloembergen, N. Conservation laws in nonlinear optics. *J. Opt. Soc. Am.* **1980**, *70*, 1429–1436.
(46) Li, L. Formulation and comparison of two recursive matrix algorithms for modeling layered diffraction gratings. *J. Opt. Soc. Am. A* **1996**, *13*, 1024–1035.
(47) Popov, E.; Mashev, L.; Maystre, D. Theoretical study of the anomalies of coated dielectric gratings. *Opt. Acta* **1986**, *33*, 607–619.
(48) Shi, Y.; Shin, W.; Fan, S. Multi-frequency finite-difference frequency-domain algorithm for active nanophotonic device simulations. *Optica* **2016**, *3*, 1256–1259.
(49) Shi, Y.; Lin, Q.; Minkov, M.; Fan, S. Nonreciprocal optical dissipation based on direction-dependent rabi splitting. *IEEE J. Sel. Top. Quantum Electron.* **2018**, *24*, 1–7.
(50) Paskov, P. P. Refractive indices of InSb, InAs, GaSb, InAs x Sb 1− x, and In 1− x Ga x Sb: effects of free carriers. *J. Appl. Phys.* **1997**, *81*, 1890–1898.
(51) Dixon, J. R.; Ellis, J. M. Optical properties of n-type indium arsenide in the fundamental absorption edge region. *Phys. Rev.* **1961**, *123*, 1560.

https://doi.org/10.1021/acsphotonics.1c01350
ACS Photonics 2022, 9, 1157–1164